

DUA-DA: Distillation-based Unbiased Alignment for Domain Adaptive Object Detection

Yongchao Feng, Shiwei Li, Yingjie Gao, Ziyue Huang, Yanan Zhang, Qingjie Liu*, Yunhong Wang
State Key Laboratory of Virtual Reality Technology and Systems, Beihang University, Beijing, China
Zhongguancun Laboratory, Beijing, China
Hangzhou Innovation Institute, Beihang University

{fengyongchao, shiweili93, gaoyingjie, ziyuehuang, zhangyanan, qingjie.liu, yhwang}@buaa.edu.cn

Abstract

Though feature-alignment based Domain Adaptive Object Detection (DAOD) have achieved remarkable progress, they ignore the source bias issue, i.e. the aligned features are more favorable towards the source domain, leading to a sub-optimal adaptation. Furthermore, the presence of domain shift between the source and target domains exacerbates the problem of inconsistent classification and localization in general detection pipelines. To overcome these challenges, we propose a novel Distillation-based Unbiased Alignment (DUA) framework for DAOD, which can distill the source features towards a more balanced position via a pre-trained teacher model during the training process, alleviating the problem of source bias effectively. In addition, we design a Target-Relevant Object Localization Network (TROLN), which can mine target-related knowledge to produce two classification-free metrics (IoU and centerness). Accordingly, we implement a Domain-aware Consistency Enhancing (DCE) strategy that utilizes these two metrics to further refine classification confidences, achieving a harmonization between classification and localization in cross-domain scenarios. Extensive experiments have been conducted to manifest the effectiveness of this method, which consistently improves the strong baseline by large margins, outperforming existing alignment-based works.

1. Introduction

State-of-the-art object detectors [25, 26, 31] have demonstrated impressive performance when the training and testing data exhibit consistent distributions. However, their performance diminishes drastically when applied to novel domains, primarily due to domain shift [4], which impedes the generalization and transferability of the detectors across different scenes. The inability of object detectors to adapt to

*Corresponding author.

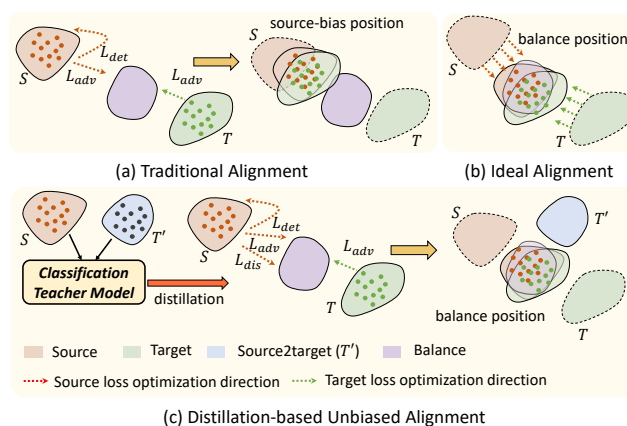


Figure 1. In (a) traditional alignment approaches, the final alignment position tends to bias towards the source domain due to the differences in optimization losses between the source and target data, rather than reaching (b) an ideal alignment position. (c) In our proposed DUA framework, by adding a distillation loss to the source data, the alignment position is compelled to be closer to a balanced position.

novel domains hampers their practical applicability in real-world scenarios.

Extensive researches have been dedicated to address the challenge via Unsupervised Domain Adaption (UDA) methods, which aim to adapt to unlabeled target domain using the annotated source domains. One of the fashionable frameworks of UDA is to align the feature distributions between the source and target domains. This class of adaptation approach performs an adversarial training of object detector models with the help of domain discriminators. Specifically, the detectors are trained to produce domain-invariant features that cannot be discriminated by the discriminator. Early works [4, 11, 14, 27] aim to align image-level and instance-level features and achieve great margins over plain detectors. Recent works [18, 30, 39]

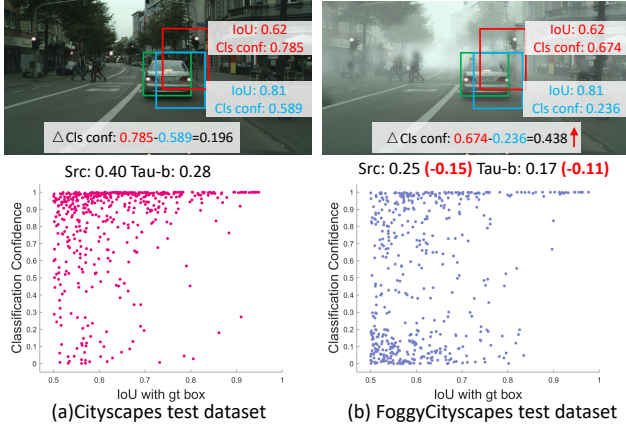


Figure 2. Demonstrative cases of the more severe inconsistency between classification and localization in the cross-domain scenarios. The upper row figures show detection results of DA-Faster [4] (trained on *Cityscapes*→*FoggyCityscapes* setting) on the *Cityscapes* and *FoggyCityscapes* test datasets. The lower row figures displays the correlation between localization ground-truth and classification scores for 500 randomly sampled detection boxes.

devote to aligning class-conditional distribution across different domains, and have achieved fine-grained adaption in a category-wise manner.

Even though, there are still two challenges in existing alignment-based methods [4, 21, 41]. Firstly, in the training phase, source data are used for simultaneously optimizing detection loss L_{det} and adversarial loss L_{adv} , while target data are solely for L_{adv} . This discrepancy in optimization losses leads to the inability of features from two domains to align to a balanced position, resulting in the source-bias issue. As illustrated in Fig. 1(a), the supervised loss L_{det} tends to preserve the distribution of the source data, while the adversarial loss L_{adv} always pulls the two domains' distributions closer together. With the combined effect of these two losses, the final alignment position tends to favor the source domain rather than an ideal alignment position (Fig. 1(b)). This significantly compromises the detectors' generalization capability in the target domain. These observations motivate us to design a new paradigm to achieve a superior alignment, compelling the aligned position to be closer to the balanced position.

The second challenge lies in the more severe inconsistency between classification and localization in cross-domain scenarios compared to original scenarios. As shown in Fig. 2(a), compared with the detected bounding box (blue), another detected bounding box (red) with higher classification scores could have lower IoU scores with ground truth boxes (green), which is defined as inconsistency between classification and localization. Furthermore, detection boxes (blue and red) located in the same position

in *FoggyCityscapes* scenario (Fig. 2(b)) often exhibit larger differences in classification scores compared with ones in *Cityscapes* (Fig. 2(a)), showcasing more severe inconsistency in the cross-domain. More generally, we randomly sampled 500 detection boxes before NMS for each scene, visualizing the correlation between classification scores (y -axis) and ground-truth localization (x -axis, defined as the IoU between the detected box and its matched ground-truth). Simultaneously, for multiple detection boxes originating from the same proposal, we retain only the one with the highest foreground class confidence. In this work, we introduce Spearman Rank Correlation Coefficient (Src) and Kendall Rank Correlation Coefficient (Tau-b) [1] to describe the consistency between the two quantities. The Src and Tau-b in the target domain are relatively lower compared to the source domain, indicating that the detector faces a more pronounced inconsistency issue in the cross-domain scenarios. Hence, we are committed to designing a cross-domain-friendly localization quality metric and employ this metric to refine classification scores, aiming to enhance the consistency between classification and localization in cross-domain scenarios.

To overcome the aforementioned constraints, we propose a novel Distillation-based Unbiased Alignment (DUA) framework. As shown in Fig. 1(c), we first transform the source images into the target domain style, named source2target domain T' (the light blue). Then we train an unbiased teacher to learn unbiased knowledge from both S and T' domain. These knowledge are utilized to guide source features' alignment in the detector's training process, compelling final alignment position to move towards the balanced position. Furthermore, we design a Target-Relevant Object Localization Network (TROLN) trained on S and T' mix-style data. Then we conduct a Domain-aware Consistency Enhancing (DCE) strategy to adjust the classification confidences of the bounding boxes based on the output of TROLN, making sure that the bounding boxes with better localization are retained.

In summary, our contributions are as follows:

- We propose a novel DUA framework for DAOD, which utilizes an unbiased classification-teacher to guide the source domain features to align towards the balanced position, encouraging the detector to learn domain-invariant feature representations.
- We conduct in-depth study of the inconsistent issue between the classification and localization in cross-domain detection. We design TROLN and conduct DCE strategy to refine classification confidences, which enhances the consistency between the classification and localization.
- Extensive experiments demonstrate that our method consistently outperforms the strong baseline by significant margins, highlighting its superiority compared to existing alignment-based methods.

2. Related Work

Domain adaptation for object detection. Several approaches have been proposed for DAOD, which can be categorized into alignment-based [4, 18, 27] and self-training [6, 24] methods. However, regardless of the technological approaches, the source bias issue persists. Self-training methods alleviate the detector’s bias towards the source domain by continuously improving the quality of pseudo-labels during training stage. The development direction of alignment-based methods often involves modeling features at a more granular level for alignment. DA-Faster [4] implements feature alignment at both the image-level and instance-level. SIGMA [18] constructs the feature distributions of the source and target domains as graphs and reformulates the adaption with graph matching. However, regardless of the granularity of modeling, it is unable to change the asymmetry in the losses between the source and target domains and cannot directly optimize the source bias problem. In this paper, we propose a novel distillation-based alignment (DUA) framework, where a distillation loss is constructed to alleviate the issue of asymmetric loss. To the best of our knowledge, this is the first method directly optimizing source bias in alignment-based approaches.

Representation of localization quality. The conflict between classification and localization tasks is a well-known problem [13, 20, 32, 38] in the object detection field. Existing works have been dedicated to finding more accurate localization metrics to guide the learning of the classification head, alleviating inconsistency issue in this way. IoU-Net [13] introduces an extra head to predict IoU and use it to rank bounding boxes in NMS. Fitness NMS [32], IoU-aware RetinaNet [35] and [29] multiply the predicted IoU or IoU-based ranking scores and the classification score as the ranking basis. Instead of predicting the IoU-based score, FCOS [31] predicts centerness scores to suppress the low-quality detections. However, in cross-domain scenarios, how to incorporate domain-relevant knowledge into localization metrics designing has become a new challenge. Unfortunately, existing methods cannot be directly applied to cross-domain scenarios. Therefore, in this paper, we propose a target-relevant OLN to mine knowledge from the target domain. And we consider domain-related context into the design of localization metrics to create a novel cross-domain-friendly localization quality metric.

3. Method

3.1. Problem Formulation

In the context of cross-domain object detection, we have a labeled source domain $\mathcal{D}_S = \{(x_i^s, y_i^s)\}_{i=1}^{N_s}$, where x_i^s and $y_i^s = (b_i^s, c_i^s)$ denote the i_{th} image and its corresponding labels, i.e., the coordinates of the bounding box b and its associated category c , respectively. In addition, we have

access to an unlabeled target domain $\mathcal{D}_T = \{x_i^t\}_{i=1}^{N_t}$. In this work, we employ CycleGAN [42] to convert the source images into the target domain style, creating a new domain named source2target domain $\mathcal{D}_{T'} = \{(x_i^{t'}, y_i^{t'})\}_{i=1}^{N_s}$, which shares labels with the source domain data. We assume that the source and target samples come from different distributions (i.e., $\mathcal{D}_S \neq \mathcal{D}_T$) but the categories are exactly the same. The objective is to enhance the performance of the detector in \mathcal{D}_T using the knowledge in \mathcal{D}_S .

3.2. Framework Overview

As shown in Fig. 3, our method involves two training stages, a teacher models training stage and an alignment training stage. In the teacher models training stage (Sec 3.3), we train a classification and a localization models as teachers using the labeled data \mathcal{D}_S and $\mathcal{D}_{T'}$. In the second training stages (Sec 3.4), the features of the positive proposals are expected to derive domain-invariant representation from the classification-teacher model. During the testing stage (Sec 3.5), we extract the localization scores from the localization-teacher (TROLN) model to refine the classification confidences, thereby alleviating the inconsistent classification and localization issue in cross-domain scenarios.

3.3. Teacher Models Training

Classification Teacher. We first construct an instance-level image dataset \mathcal{D} as image corpus by extracting all class objects from the detection dataset \mathcal{D}_S and $\mathcal{D}_{T'}$ according to their ground-truth bounding boxes and labels. Formally, given an image corpus \mathcal{D} , for an image $I \in \mathcal{D}$, we first perform typical data augmentations (random cropping, color distortion, etc.) to obtain I' . Then we feed the augmented image I' into a ResNet [8] classification network for supervised learning. Since \mathcal{D} contains images with two different domain styles, this classifier can effectively map the input images to a domain-balanced feature distribution.

TROLN Teacher. To capture target-relevant knowledge from both \mathcal{D}_S and $\mathcal{D}_{T'}$ and refine the classification scores of \mathcal{D}_T for enhancing the consistency between classification and localization, we propose a Target-Relevant Object Localization Network. The original OLN [16] estimates the objectness of each region by centerness-head and IoU-head. The comprehensive loss function of OLN can be written as:

$$\begin{aligned} \mathcal{L}_{OLN} &= \mathcal{L}_{RPN}^{Cent} + \mathcal{L}_{RPN}^{reg} + \mathcal{L}_{RCNN}^{IoU} + \mathcal{L}_{RCNN}^{reg} \\ \mathcal{L}_{RPN}^{Cent} &= \frac{1}{N_{pix}} \sum_{x=1}^W \sum_{y=1}^H \mathcal{K}_{for}^{pix} L_1(c_{x,y}, \hat{c}_{x,y}) \\ \mathcal{L}_{RCNN}^{IoU} &= \frac{1}{N_{pos}} \sum_{r=1}^{N_{pos}} \mathcal{K}_{for}^{pro} L_1(b_r, \hat{b}_r) \end{aligned} \quad (1)$$

where \mathcal{K}_{for}^{pix} and \mathcal{K}_{for}^{pro} denote the positive pixels and positive proposals set. $c_{x,y}$, b_r , $\hat{c}_{x,y}$, \hat{b}_r are the predicted center-

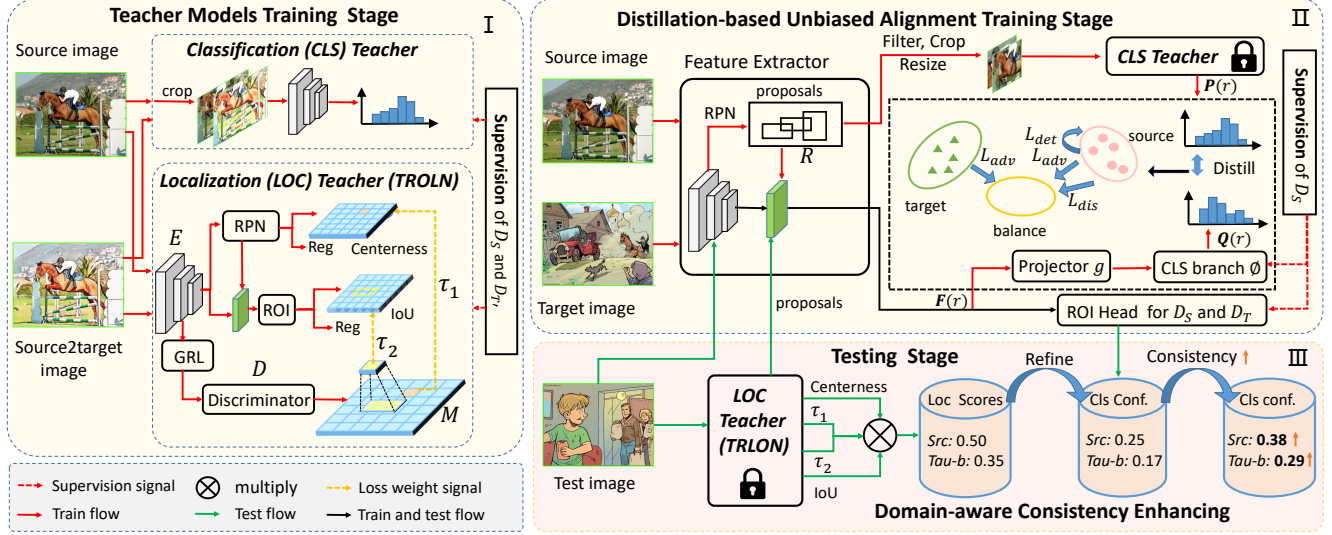


Figure 3. Overview of the proposed distillation-based unbiased alignment framework for DAOD. Part I shows the teacher models training stage, which includes a mix-style classifier and a Target-Relevant object localization network (TROLN) training. Part II demonstrates distillation-based unbiased alignment (DUA) training, in which the cross-domain detector is trained. In Part III, the Domain-aware Consistency Enhancement (DCE) strategy is introduced to refine the detector’s classification scores in the testing phase, enhancing the consistency between classification and localization in cross-domain scenarios.

ness, predicted IoU, groundtruth centerness and groundtruth IoU, respectively.

When combining S and T' data to train OLN, the lack of guidance from the target domain results in less relevant images being given the same importance as more relevant ones, leading to a deterioration in knowledge learning and mining from the target domain. To address this issue, TROLN has been developed to ensure that target-relevant knowledge are encoded at the pixel and instance level by assigning target-relevant weights τ_1 and τ_2 to each centerness-loss and IoU-loss item. Specifically, a pixel-level domain discriminator D is placed after the feature encoder E (shown in Fig. 3 I) in the TROLN. The discriminator’s purpose is to distinguish whether the derived feature $E(X) \in \mathbb{R}^{H \times W \times C}$ is from S or T' , where H , W and C denote the height, width and channel of the feature map, respectively. The probability of each pixel belonging to the target domain is defined as $D(E(X)) \in \mathbb{R}^{H \times W \times 1}$ and $1 - D(E(X)) \in \mathbb{R}^{H \times W \times 1}$ represents the probability of it belonging to the source domain. The domain discriminator D is updated using binary cross-entropy loss based on the domain label d for each input image, where images from the source domain are labeled as $d = 0$ and images from target domain are labeled as $d = 1$. The discriminator loss \mathcal{L}_{dis} can be expressed as:

$$\mathcal{L}_{dis} = -d \log D(E(X)) - (1 - d) \log(1 - D(E(X))) \quad (2)$$

The large value within $D(E(X))$ indicates that the distribution of current pixel and target pixels are more similar. Based on the important cues, we denote $D(E(X))$ as target affinity score map M and design dynamic domain-related loss to weight the \mathcal{L}_{RPN}^{Cent} and \mathcal{L}_{RCNN}^{IoU} . As shown in Eq. 3, pixel-level domain affinity weight τ_1 is defined as the value at the coordinate (x, y) and instance-level domain affinity weight τ_2 is denoted as the average of ROIAlign based on the T and corresponding proposal p .

$$\begin{aligned} \tau_1 &= M(x, y) \\ \tau_2 &= \text{Average}(\text{ROIAlign}(M, p)) \end{aligned} \quad (3)$$

Subsequently, we can re-weight the importance of loss items from pixel and instance level as illustrated in Fig. 3 I, and apply it to train a localization-teacher (TROLN) by reformulating the loss function in Eq. 1 as the following:

$$\begin{aligned} \mathcal{L}_{TROLN} &= \mathcal{L}_{RPN}^{Cent} + \mathcal{L}_{RPN}^{reg} + \mathcal{L}_{RCNN}^{IoU} + \mathcal{L}_{RCNN}^{reg} + \mathcal{L}_{dis} \\ \mathcal{L}_{RPN}^{Cent} &= \frac{1}{N_{pix}} \sum_{x=1}^W \sum_{y=1}^H \mathcal{K}_{for}^{pix}(\tau_1 + 1) L_1(c_{x,y}, \hat{c}_{x,y}) \\ \mathcal{L}_{RCNN}^{IoU} &= \frac{1}{N_{pos}} \sum_{r=1}^{N_{pos}} \mathcal{K}_{for}^{pro}(\tau_2 + 1) L_1(b_r, \hat{b}_r) \end{aligned} \quad (4)$$

Based on Eq. 4, TROLN is explicitly enforced to learn from target-relevant samples, and thus prevents the interference from the information irrelevant to the target.

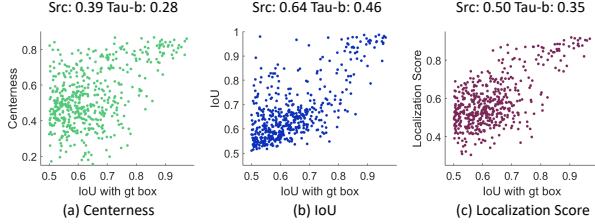


Figure 4. The correlation between localization ground-truth and centerness/IoU/localization scores of the detected boxes on the target test dataset. The detected boxes all have an IoU (≥ 0.5) with the corresponding ground-truth.

3.4. Distillation-based Unbiased Alignment

Our classification-teacher model is optimized based on the mixed-style dataset \mathcal{D} in a completely independent way from the object detection. As a result, the encoded feature of an image in the teacher model’s embedding space can be viewed as domain-invariant knowledge. These knowledge can be transferred to the learning process of object detection to suppress potential source bias. The rationale behind this design is that a non-bias representations of an object category learned by a detector should bear consistent distribution with that learned by the classification-teacher model.

In the DUA training stage, we use DA-Faster [4] as our base detector and its training loss is noted as \mathcal{L}_{DA} . As shown in Fig. 3 II, in the DUA training stage, given proposals R generated by RPN, we first filter out R with an IOU higher than T (0.8) with the ground-truth boxes. Then we crop the corresponding regions from the source image and resize them to a fixed size using bilinear interpolation, then feed them into our classification-teacher model to obtain their classification logit $\mathbf{P}(r) \in \mathbb{R}^{K \times 1}$. Here, K represents the number of classes in the object detection task, r represents one of proposals in filtered results. Meanwhile, we obtain the ROI features $\mathbf{F}(r)$ for r from the RoI Align layer of the object detector. Note that $\mathbf{F}(r)$ and $\mathbf{P}(r)$ are learned in the different feature space, thus we first project $\mathbf{F}(r)$ into the same feature space as $\mathbf{P}(r)$ and then obtain the classification logit of the projected feature:

$$\mathbf{Q}(r) = \phi(g(\mathbf{F}(r))) \quad (5)$$

Here, $g(\cdot)$ denotes the project function for features $\mathbf{F}(r)$, which is implemented with a 1×1 convolutional layer, while $\phi(\cdot)$ is the classification branch in the detection head. Then we minimize the L1-norm between these two logit representations to guide the learning process of the detector:

$$L_{\text{dist}} = \frac{1}{RK} \sum_{r=1}^R \sum_{k=1}^K \|\mathbf{P}_k(r) - \mathbf{Q}_k(r)\|_1 \quad (6)$$

where R is the number of positive proposals. The obtained logit representation $\mathbf{Q}(r)$ can also be utilized for classifica-

tion of the region proposal r . Thus, we conduct an auxiliary classification on the logit $\mathbf{Q}(r)$.

$$\begin{aligned} p' &= \mathcal{F}_{\text{softmax}}(\mathbf{Q}(r)) \\ \mathcal{L}_{\text{cls-aux}} &= \text{CE}(y, p'), \end{aligned} \quad (7)$$

where p' is the predicted scores based on $\mathbf{Q}(r)$, y is the groundtruth label for the region proposal r . Note that the whole distillation process is only conducted on the source images.

Consequently, the object detector is trained under the supervision of the three losses jointly:

$$\mathcal{L}_{\text{obj}} = \mathcal{L}_{DA} + \lambda_1 \mathcal{L}_{\text{dist}} + \lambda_2 \mathcal{L}_{\text{cls-aux}}, \quad (8)$$

λ_1 and λ_2 are trade-off parameters to balance the domain adaption, distillation loss and auxiliary loss.

3.5. Domain-aware Consistency Enhancing

To address more severe inconsistency between classification and localization in the cross-domain scenarios, we attempt to design a novel cross-domain-friendly localization metric to refine classification scores, enhancing the consistency between classification and localization. Since TROLN has already explored the target-relevant localization knowledge, we first investigate the relation between localization ground-truths and two class-agnostic metrics (IoU and centerness) based on TROLN.

In the TROLN framework, we consider that these three share the same centerness and IoU. Similar to Fig. 2, we evaluate the trained TROLN on the FoggyCityscapes test datasets and visualize the correlation of two metrics (y -axis, centerness and IoU) and ground-truth localization (x -axis), as shown in Fig. 4(a) and (b). It is evident that compared to the classification score in Fig. 2(b), both IoU and centerness exhibit a higher consistency with the localization ground truths. This indicates that these two metrics have the potential to serve as localization indicators for refining the classification confidences.

However, using the highest consistency metric (IoU) to weight the classification confidences could cause an extra class confusion issue. For example, if two detected boxes simultaneously match the same ground truth box with the category “cat”, where the detected box A predicts a “cat” confidence of 0.6 and an IoU of 0.5, and detected box B predicts a “tiger” confidence of 0.5 and an IoU of 0.7. In this case, employing the IoU to weigh classification confidence would yield a “cat” confidence of 0.3 (0.6×0.5) for detected box A and a “tiger” confidence of 0.35 (0.5×0.7) for detected box B , potentially resulting in misclassification. On the other hand, refining classification confidence based on centerness may not sufficiently improve the consistency between the classification and the localization ground truths. Although centerness and IoU already incorporate



Figure 5. The correlation changes between the refined classification confidences and the localization ground truth of the detected boxes among various classes, before and after the refinement.

target-relevant knowledge, they cannot adaptively adjust to domain-aware information. Therefore, we incorporate pixel and instance-level domain affinity weight τ_1 , τ_2 into the localization metrics and strike a balance between centerness and IoU. Here, we propose a novel domain-aware localization score s as the following:

$$s = \sqrt{4 \times c \times b \times \tau_1 \times \tau_2}, \quad (9)$$

where c and b denote centerness and IoU, respectively. Here, s exhibits a high consistency with the localization ground-truth (Fig. 4(c)).

Then we use s to refine classification scores to enhance the consistency between the classification and localization, which is referred to as Domain-aware Consistency Enhancing strategy. Concretely, in the testing stage, given an image I , we feed it to the TROLN to obtain a proposals set $\mathcal{R} = \{(box_i, s_i)\}_{i=1}^{N_p}$, where box_i and s_i represent the spatial coordinates and the localization score of the i -th proposal. N_p denotes the total number of proposals. Simultaneously, we feed I into the trained detector, replacing the detector’s proposals with \mathcal{R} . As a result, we obtain the ROI head output $\mathcal{T} = \{(reg_i, cls_i)\}_{i=1}^{N_p}$, where reg_i and cls_i denote the regression results and classification scores respectively. Finally, following Eq. 10, we utilize s_i to refine cls_i , and obtain the adjusted classification score cls'_i :

$$cls'_i = \mathcal{F}_{\text{softmax}} \sqrt[4]{cls_i \times s_i} \quad (10)$$

The refined output $\mathcal{T}' = \{(reg_i, cls'_i)\}_{i=1}^{N_p}$ are used to participate NMS and evaluate the performance by following DA-Faster [4] protocol.

4. Experiments

4.1. Datasets and Implementation Details

We conduct our experiments on four datasets, including (1) *Cityscapes* [5] contains authentic urban street scenes

captured under normal weather conditions, encompassing 2,975 training images and 500 validation images with detailed pixel-level annotations. (2) *FoggyCityscapes* [28] is a derivative dataset that simulates dense foggy conditions based on *Cityscapes*, maintaining the same train/validation split and annotations. (3) *KITTI* [7] is another popular dataset for autonomous driving. It consists of 7,481 labeled images for training. (4) *SIM10k* [15] is a synthetic dataset containing 10,000 images rendered from the video game Grand Theft Auto V (GTA5).

We report AP_{50} of each class for object detection following [4] for all of the experimental setting, which are described as follows: (1) *Cityscapes* \rightarrow *FoggyCityscapes*. It aims to perform adaptation across different weather conditions. (2) *Kitti* \rightarrow *Cityscapes*. It is cross camera adaption, where the source and target domain data are captured with different camera setups. (3) *SIM10k* \rightarrow *Cityscapes*. To adapt the synthetic scenes to the real one, we utilize the entire *SIM10k* dataset as the source domain and the training set of *Cityscapes* as the target domain. Following [19], we only report the performance on car for the last two scenarios.

We employ DA-Faster [4] and AT [21] as the base detection model. In the DUA training stage, we resize all the images (crop according to proposals) to 224×224 , and the proposals’ IoU threshold $T = 0.8$. For the hyperparameter, we set the $\lambda_1 = 1.0$ and $\lambda_2 = 1.0$ for all the experiments. We trained the detector (DA-Faster) with SGD optimizer with a 0.001 learning rate, 2 batch size, momentum of 0.9, and weight decay of 0.0005 for 70k iterations. Each experiment is conducted on 1 Nvidia GPU 2080Ti or 4 Nvidia GPU 3090 when base detection model is DA-Faster or AT. For more detailed experimental details, please refer to the supplementary materials.

4.2. Results

Cityscapes \rightarrow *FoggyCityscapes*. We present the comparison with VGG16, ResNet50 and ResNet101 backbones in Table 1. When base detector is DA-Faster, our method achieves 44.2%, 45.2%, and 45.7% mAP, respectively, improving mAP by 0.7%, 4.3% and 3.5% comparing with the state-of-the-art on different backbone settings. Simultaneously, our method has achieved consistent improvements on AT and CMT as well. This fully demonstrates the effectiveness of our approach and its compatibility with the different backbone networks.

Kitti \rightarrow *Cityscapes*. In Table 2, we illustrate the performance comparison on the cross-camera task. The proposed method reaches an AP_{50} of 46.9% and 49.3% with a gain of +12.4% and +14.8% over the SO model with different base detector, respectively.

SIM10k \rightarrow *Cityscapes*. Table 3 shows that our method consistently improves performance across different base detectors. This further illustrates that the proposed approach

Table 1. Results from Cityscapes to Foggy Cityscapes.

Method	Backbone	person	rider	car	truck	bus	train	mcycle	bcycle	mAP
SWDA [27]	VGG16	36.2	35.3	43.5	30.0	29.9	42.3	32.6	24.5	34.3
Selective DA [43]		33.5	38.0	48.5	26.5	39.0	23.3	28.0	33.6	33.8
DD-MRL [17]		30.8	40.5	44.3	27.2	38.4	34.5	28.4	32.2	34.5
CRDA [36]		32.9	43.8	49.2	27.2	45.1	36.4	30.3	34.6	37.4
CFFA [41]		34.0	46.9	52.1	30.8	43.2	29.9	34.7	37.4	38.6
ATF [10]		34.6	47.0	50.0	23.7	43.3	38.7	33.4	38.8	38.7
MCAR [40]		32.0	42.1	43.9	31.3	44.1	43.4	37.4	36.6	38.8
HTCN [3]		33.2	47.5	47.9	31.6	47.4	40.9	32.3	37.1	39.8
MeGA [33]		37.7	49.0	52.4	25.4	49.2	46.9	34.5	39.0	41.8
SSAL [23]		45.1	47.4	59.4	24.5	50.0	25.7	26.0	38.7	39.6
SIGMA [18]		46.9	48.4	63.7	27.1	50.7	35.9	34.7	41.4	43.5
DUA-DA (Ours)		46.5	54.1	61.9	28.3	49.5	26.7	40.0	46.3	44.2
AT [21]	VGG16	45.3	55.7	63.6	36.8	64.9	34.9	42.1	51.3	49.3
AT [21] + DUA-DA		49.1	59.3	66.2	35.8	60.0	47.1	45.2	54.9	52.2
CMT [2]		45.9	55.7	63.7	39.6	66.0	38.8	41.4	51.2	50.3
CMT [2] + DUA-DA		49.0	59.6	65.3	35.7	61.0	46.5	43.9	57.3	52.3
GPA [37]	ResNet50	32.9	46.7	54.1	24.7	45.7	41.1	32.4	38.7	39.5
CRDA [36]		39.9	38.1	57.3	28.7	50.7	37.2	30.2	34.2	39.5
DIDN [22]		38.3	44.4	51.8	28.7	53.3	34.7	32.4	40.4	40.5
DSS [34]		42.9	51.2	53.6	33.6	49.2	18.9	36.2	41.8	40.9
DUA-DA (Ours)		43.7	49.1	60.7	30.8	55.7	43.4	33.7	44.6	45.2
CADA [11]	ResNet101	41.5	43.6	57.1	29.4	44.9	39.7	29.0	36.1	40.2
D-adapt [14]		42.8	48.4	56.8	31.5	42.8	37.4	35.2	42.4	42.2
DUA-DA (Ours)		43.9	50.7	61.6	31.8	52.2	47.1	32.1	46.1	45.7

Table 2. Results on KITTI to Cityscapes with VGG-16. SO represents the source only results and GAIN indicates the adaption gains compared with the source only model.

Method	Car	SO/GAIN
CADA [11]	43.2	34.4/ 8.8
DSS [34]	42.7	34.6/ 8.1
MEGA [33]	43.0	30.2/ 12.8
SSAL [23]	45.6	34.9/ 10.7
KTNet [30]	45.6	34.4/ 11.2
SIGMA [18]	45.8	34.4/ 11.4
DUA-DA (Ours)	46.9	34.5/ 12.4
AT [21]	47.7	34.4/ 13.3
AT [21]+ DUA-DA	49.3	34.5/ 14.8

has strong generalization capabilities, effectively adapting from synthetic to real setting.

4.3. Source Bias Measure

In this section, we endeavor to quantitatively measure the degree of source bias in the model, thereby demonstrating the effectiveness of the DUA module. Due to the fact that the features before and after alignment originate from dif-

Table 3. Results from Sim10k to Cityscapes.

Method	Car	SO/GAIN
SWDA [12]	40.1	34.3/ 5.8
MAF [9]	41.1	34.3/ 6.8
Selective DA [43]	43.0	34.3/ 8.7
HTCN [3]	42.5	34.4/ 8.1
CFFA [41]	43.8	34.3/ 9.5
ATF [10]	42.8	34.3/ 8.5
MeGA-CDA [33]	44.8	34.3/ 10.5
UMT [6]	43.1	34.3/ 8.8
DUA-DA (Ours)	47.8	34.6/ 13.2
AT [21]	51.4	34.6/ 16.8
AT [21] + DUA-DA	52.5	34.6/ 17.9

ferent models, it is not possible to directly measure source bias by comparing the distance of feature distributions in different feature spaces. Here, we evaluate the performance disparity of the model between the source and target domains as an indirect reflection of the degree of source bias. The rationale behind this design is that a non-bias model should exhibit consistent performance on both the source and target domains, i.e., $AP_s = AP_t$.

Table 4. Source bias among different models under various backbones.

Method	Backbone	$AP_s \uparrow$	$AP_t \uparrow$	$\Theta \downarrow$
Source Only	VGG16	49.02	20.18	41.68%
Baseline		48.91	39.56	10.57%
Baseline+DUA		50.09	42.00	8.78%
Source Only	Resnet50	50.12	23.92	35.39%
Baseline		50.21	40.90	10.22%
Baseline+DUA		51.48	43.05	8.91%

Table 5. Ablation study on the proposed DUA and DCE.

Module		mAP		
DUA	DCE	VGG16	ResNet50	ReNet101
		39.56	40.15	41.09
✓		42.00	43.05	42.63
	✓	42.14	43.23	43.11
✓	✓	44.21	45.22	45.73

More specifically, we employ Eq. 11 to define the degree of source bias. The reason can be summarized into two aspects: 1) As the model’s performance become more similar on the S and T , Θ becomes smaller. 2) when the performance disparity remains constant between the two domains but the overall performance in both domains improves, Θ also decreases. Therefore, Θ serves as a more comprehensive metric reflecting the model’s source bias.

$$\Theta = \frac{|AP_s - AP_t|}{AP_s + AP_t} \quad (11)$$

As shown in Table 4, compared with the Source Only, Baseline and Ours reduce the Θ by large margins, which demonstrates the positive impact of feature alignment in reducing source bias. Further, since we conduct DUA strategy which distill domain-invariant knowledge to the detector, compelling the aligned position to be closer to the balanced position, we achieve a smaller Θ compared to Baseline.

4.4. Ablation Study

In this section, we conduct ablation studies to validate our contributions. All experiments are conducted on the *FoggyCityscapes* validation set. For more ablation experiments and analysis regarding our method, please refer to the supplementary materials.

Effectiveness of each component. We first investigate the impact of DUA and DCE on the final results. As shown in Table 5, both DUA and DCE can improve the performance of the baseline under different backbone configurations. Finally, with all these components, we increase the mAP of the baseline by 4.65%, 5.07% and 4.64% respectively, when using Resnet50, Resnet101 and VGG16 as

Table 6. Ablation experiments on the TROLN and DCE.

TROLN Training Stage				DCE Testing Stage				
c	b	τ_1	τ_2	c	b	τ_1	τ_2	AP_{50}
								43.05
✓	✓			✓				43.95
✓	✓				✓			43.98
✓	✓			✓	✓			44.12
✓	✓	✓	✓	✓	✓			44.76
✓	✓	✓	✓	✓	✓	✓	✓	45.22

backbones. This demonstrates the effectiveness and necessity of DUA and DCE.

Choose of localization metric. For brevity, we refer to centerness and IoU as c and b . Here, we attempt to conduct ablation experiments on the training strategy of TROLN and the testing strategy of DCE. As shown in Table 6, when we only use c and b to train TROLN (original OLN), using either c , b , or $\sqrt{c \times b}$ as localization metric to refine classification scores can all improve the model’s performance to varying degrees. This indicates that enhancing the consistency between classification and localization can effectively improve the detector’s performance. Furthermore, when training with TROLN (ours), using the cross-domain-friendly localization score ($\sqrt{4 \times c \times b \times \tau_1 \times \tau_2}$) as the localization metric to calibrate classification scores, the model achieves the highest performance improvement (+2.17% compared with baseline). This further validates the necessity and effectiveness of the TROLN training strategy and the DCE testing strategy. Moreover, we evaluate the consistency between the classification confidences in different classes and the localization ground-truth before and after refinement on the test dataset. As shown in Fig. 5, it can be observed that the consistency between classification and localization has been improved to varying degrees across almost all categories, further demonstrating the effectiveness of the DCE mechanism.

5. Conclusion

To address source bias issue in domain adaptive object detection, we propose a distillation-based unbiased alignment framework. We train an instance-level classification-teacher model to calibrate source features distribution, compelling source features to align to a more balanced position. We also design a cross-domain-friendly localization metric to refine classification confidences, further improving the performance of the detector. Finally, our method achieved considerable improvement on several benchmark datasets under different base detectors for domain adaptation, demonstrating the effectiveness.

References

- [1] Hervé Abdi. The kendall rank correlation coefficient. *Encyclopedia of Measurement and Statistics*. Sage, Thousand Oaks, CA, pages 508–510, 2007. [2](#)
- [2] Shengcao Cao, Dhiraj Joshi, Liang-Yan Gui, and Yu-Xiong Wang. Contrastive mean teacher for domain adaptive object detectors. In *Proceedings of the IEEE/CVF Conference on Computer Vision and Pattern Recognition*, pages 23839–23848, 2023. [7](#)
- [3] Chaoqi Chen, Zebiao Zheng, Xinghao Ding, Yue Huang, and Qi Dou. Harmonizing transferability and discriminability for adapting object detectors. In *Proceedings of the IEEE/CVF Conference on Computer Vision and Pattern Recognition*, pages 8869–8878, 2020. [7](#)
- [4] Yuhua Chen, Wen Li, Christos Sakaridis, Dengxin Dai, and Luc Van Gool. Domain adaptive faster r-cnn for object detection in the wild. In *Proceedings of the IEEE Conference on Computer Vision and Pattern Recognition*, pages 3339–3348, 2018. [1](#), [2](#), [3](#), [5](#), [6](#)
- [5] Marius Cordts, Mohamed Omran, Sebastian Ramos, Timo Rehfeld, Markus Enzweiler, Rodrigo Benenson, Uwe Franke, Stefan Roth, and Bernt Schiele. The cityscapes dataset for semantic urban scene understanding. In *Proceedings of the IEEE Conference on Computer Vision and Pattern Recognition*, pages 3213–3223, 2016. [6](#)
- [6] Jinhong Deng, Wen Li, Yuhua Chen, and Lixin Duan. Unbiased mean teacher for cross-domain object detection. In *Proceedings of the IEEE/CVF Conference on Computer Vision and Pattern Recognition*, pages 4091–4101, 2021. [3](#), [7](#)
- [7] Andreas Geiger, Philip Lenz, and Raquel Urtasun. Are we ready for autonomous driving? the kitti vision benchmark suite. In *2012 IEEE Conference on Computer Vision and Pattern Recognition*, pages 3354–3361. IEEE, 2012. [6](#)
- [8] Kaiming He, Xiangyu Zhang, Shaoqing Ren, and Jian Sun. Deep residual learning for image recognition. In *Proceedings of the IEEE Conference on Computer Vision and Pattern Recognition*, pages 770–778, 2016. [3](#)
- [9] Zhenwei He and Lei Zhang. Multi-adversarial faster-rcnn for unrestricted object detection. In *Proceedings of the IEEE/CVF International Conference on Computer Vision*, pages 6668–6677, 2019. [7](#)
- [10] Zhenwei He and Lei Zhang. Domain adaptive object detection via asymmetric tri-way faster-rcnn. In *Computer Vision—ECCV 2020: 16th European Conference, Glasgow, UK, August 23–28, 2020, Proceedings, Part XXIV 16*, pages 309–324. Springer, 2020. [7](#)
- [11] Cheng-Chun Hsu, Yi-Hsuan Tsai, Yen-Yu Lin, and Ming-Hsuan Yang. Every pixel matters: Center-aware feature alignment for domain adaptive object detector. In *Computer Vision—ECCV 2020: 16th European Conference, Glasgow, UK, August 23–28, 2020, Proceedings, Part IX 16*, pages 733–748. Springer, 2020. [1](#), [7](#)
- [12] Naoto Inoue, Ryosuke Furuta, Toshihiko Yamasaki, and Kiyoharu Aizawa. Cross-domain weakly-supervised object detection through progressive domain adaptation. In *Proceedings of the IEEE Conference on Computer Vision and Pattern Recognition*, pages 5001–5009, 2018. [7](#)
- [13] Borui Jiang, Ruixuan Luo, Jiayuan Mao, Tete Xiao, and Yunqing Jiang. Acquisition of localization confidence for accurate object detection. In *Proceedings of the European Conference on Computer Vision*, pages 784–799, 2018. [3](#)
- [14] Jinguang Jiang, Baixu Chen, Jianmin Wang, and Mingsheng Long. Decoupled adaptation for cross-domain object detection. *arXiv preprint arXiv:2110.02578*, 2021. [1](#), [7](#)
- [15] Matthew Johnson-Roberson, Charles Barto, Rounak Mehta, Sharath Nittur Sridhar, Karl Rosaen, and Ram Vasudevan. Driving in the matrix: Can virtual worlds replace human-generated annotations for real world tasks? *arXiv preprint arXiv:1610.01983*, 2016. [6](#)
- [16] Dahun Kim, Tsung-Yi Lin, Anelia Angelova, In So Kweon, and Weicheng Kuo. Learning open-world object proposals without learning to classify. *IEEE Robotics and Automation Letters*, 7(2):5453–5460, 2022. [3](#)
- [17] Taekyung Kim, Minki Jeong, Seunghyeon Kim, Seokeon Choi, and Changick Kim. Diversify and match: A domain adaptive representation learning paradigm for object detection. In *Proceedings of the IEEE/CVF Conference on Computer Vision and Pattern Recognition*, pages 12456–12465, 2019. [7](#)
- [18] Wuyang Li, Xinyu Liu, and Yixuan Yuan. Sigma: Semantic-complete graph matching for domain adaptive object detection. In *Proceedings of the IEEE/CVF Conference on Computer Vision and Pattern Recognition*, pages 5291–5300, 2022. [1](#), [3](#), [7](#)
- [19] Wuyang Li, Xinyu Liu, and Yixuan Yuan. Sigma++: Improved semantic-complete graph matching for domain adaptive object detection. *IEEE Transactions on Pattern Analysis and Machine Intelligence*, 2023. [6](#)
- [20] Xiang Li, Wenhai Wang, Lijun Wu, Shuo Chen, Xiaolin Hu, Jun Li, Jinhui Tang, and Jian Yang. Generalized focal loss: Learning qualified and distributed bounding boxes for dense object detection. In *Proceedings of the Advances in Neural Information Processing Systems*, pages 21002–21012, 2020. [3](#)
- [21] Yu-Jhe Li, Xiaoliang Dai, Chih-Yao Ma, Yen-Cheng Liu, Kan Chen, Bichen Wu, Zijian He, Kris Kitani, and Peter Vajda. Cross-domain adaptive teacher for object detection. In *Proceedings of the IEEE/CVF Conference on Computer Vision and Pattern Recognition*, pages 7581–7590, 2022. [2](#), [6](#), [7](#)
- [22] Chuang Lin, Zehuan Yuan, Sicheng Zhao, Peize Sun, Changhu Wang, and Jianfei Cai. Domain-invariant disentangled network for generalizable object detection. In *Proceedings of the IEEE/CVF International Conference on Computer Vision*, pages 8771–8780, 2021. [7](#)
- [23] Muhammad Akhtar Munir, Muhammad Haris Khan, M Sarfraz, and Mohsen Ali. Ssal: Synergizing between self-training and adversarial learning for domain adaptive object detection. In *Proceedings of the Advances in Neural Information Processing Systems*, pages 22770–22782, 2021. [7](#)
- [24] Rindra Ramamonjison, Amin Banitalebi-Dehkordi, Xinyu Kang, Xiaolong Bai, and Yong Zhang. Simrod: A simple

- adaptation method for robust object detection. In *Proceedings of the IEEE/CVF International Conference on Computer Vision*, pages 3570–3579, 2021. 3
- [25] Joseph Redmon and Ali Farhadi. Yolov3: An incremental improvement. *arXiv preprint arXiv:1804.02767*, 2018. 1
- [26] Shaoqing Ren, Kaiming He, Ross Girshick, and Jian Sun. Faster r-cnn: Towards real-time object detection with region proposal networks. In *Proceedings of the Advances in Neural Information Processing Systems*, 2015. 1
- [27] Kuniaki Saito, Yoshitaka Ushiku, Tatsuya Harada, and Kate Saenko. Strong-weak distribution alignment for adaptive object detection. In *Proceedings of the IEEE/CVF Conference on Computer Vision and Pattern Recognition*, pages 6956–6965, 2019. 1, 3, 7
- [28] Christos Sakaridis, Dengxin Dai, and Luc Van Gool. Semantic foggy scene understanding with synthetic data. *International Journal of Computer Vision*, 126:973–992, 2018. 6
- [29] Zhiyu Tan, Xuecheng Nie, Qi Qian, Nan Li, and Hao Li. Learning to rank proposals for object detection. In *Proceedings of the IEEE/CVF International Conference on Computer Vision*, pages 8273–8281, 2019. 3
- [30] Kun Tian, Chenghao Zhang, Ying Wang, Shiming Xiang, and Chunhong Pan. Knowledge mining and transferring for domain adaptive object detection. In *Proceedings of the IEEE/CVF International Conference on Computer Vision*, pages 9133–9142, 2021. 1, 7
- [31] Zhi Tian, Chunhua Shen, Hao Chen, and Tong He. Fcos: Fully convolutional one-stage object detection. In *Proceedings of the IEEE/CVF International Conference on Computer Vision*, pages 9627–9636, 2019. 1, 3
- [32] Lachlan Tychsen-Smith and Lars Petersson. Improving object localization with fitness nms and bounded iou loss. In *Proceedings of the IEEE Conference on Computer Vision and Pattern Recognition*, pages 6877–6885, 2018. 3
- [33] Vibashan Vs, Vikram Gupta, Poojan Oza, Vishwanath A Sindagi, and Vishal M Patel. Mega-cda: Memory guided attention for category-aware unsupervised domain adaptive object detection. In *Proceedings of the IEEE/CVF Conference on Computer Vision and Pattern Recognition*, pages 4516–4526, 2021. 7
- [34] Yu Wang, Rui Zhang, Shuo Zhang, Miao Li, YangYang Xia, XiShan Zhang, and ShaoLi Liu. Domain-specific suppression for adaptive object detection. In *Proceedings of the IEEE/CVF Conference on Computer Vision and Pattern Recognition*, pages 9603–9612, 2021. 7
- [35] Shengkai Wu, Xiaoping Li, and Xinggang Wang. Iou-aware single-stage object detector for accurate localization. *Image and Vision Computing*, 97:103911, 2020. 3
- [36] Chang-Dong Xu, Xing-Ran Zhao, Xin Jin, and Xiu-Shen Wei. Exploring categorical regularization for domain adaptive object detection. In *Proceedings of the IEEE/CVF Conference on Computer Vision and Pattern Recognition*, pages 11724–11733, 2020. 7
- [37] Minghao Xu, Hang Wang, Bingbing Ni, Qi Tian, and Wenjun Zhang. Cross-domain detection via graph-induced prototype alignment. In *Proceedings of the IEEE/CVF Conference on Computer Vision and Pattern Recognition*, pages 12355–12364, 2020. 7
- [38] Haoyang Zhang, Ying Wang, Feras Dayoub, and Niko Sunderhauf. Varifocalnet: An iou-aware dense object detector. In *Proceedings of the IEEE/CVF Conference on Computer Vision and Pattern Recognition*, pages 8514–8523, 2021. 3
- [39] Yixin Zhang, Zilei Wang, and Yushi Mao. Rpn prototype alignment for domain adaptive object detector. In *Proceedings of the IEEE/CVF Conference on Computer Vision and Pattern Recognition*, pages 12425–12434, 2021. 1
- [40] Zhen Zhao, Yuhong Guo, Haifeng Shen, and Jieping Ye. Adaptive object detection with dual multi-label prediction. In *Computer Vision—ECCV 2020: 16th European Conference, Glasgow, UK, August 23–28, 2020, Proceedings, Part XXVIII 16*, pages 54–69. Springer, 2020. 7
- [41] Yangtao Zheng, Di Huang, Songtao Liu, and Yunhong Wang. Cross-domain object detection through coarse-to-fine feature adaptation. In *Proceedings of the IEEE/CVF Conference on Computer Vision and Pattern Recognition*, pages 13766–13775, 2020. 2, 7
- [42] Jun-Yan Zhu, Taesung Park, Phillip Isola, and Alexei A Efros. Unpaired image-to-image translation using cycle-consistent adversarial networks. In *Proceedings of the IEEE International Conference on Computer Vision*, pages 2223–2232, 2017. 3
- [43] Xinge Zhu, Jiangmiao Pang, Ceyuan Yang, Jianping Shi, and Dahua Lin. Adapting object detectors via selective cross-domain alignment. In *Proceedings of the IEEE/CVF Conference on Computer Vision and Pattern Recognition*, pages 687–696, 2019. 7